Broadband Reflector Based on Double-Layer Subwavelength Gratings

Qi Wang (shelly3030@163.com)
University of Shanghai for Science and Technology School of Optical-Electrical and Computer Engineering https://orcid.org/0000-0002-8468-6024

Rui Li
University of Shanghai for Science and Technology School of Optical-Electrical and Computer Engineering

Xufeng Gao
University of Shanghai for Science and Technology School of Optical-Electrical and Computer Engineering

Shuhua Cao
University of Shanghai for Science and Technology School of Optical-Electrical and Computer Engineering

Chunxian Tao
University of Shanghai for Science and Technology School of Optical-Electrical and Computer Engineering

Ruijin Hong
University of Shanghai for Science and Technology School of Optical-Electrical and Computer Engineering

Dawei Zhang
University of Shanghai for Science and Technology School of Optical-Electrical and Computer Engineering

Research Article

Keywords: broadband reflector, guided mode resonance, double-layer grating

Posted Date: March 25th, 2021

DOI: https://doi.org/10.21203/rs.3.rs-343925/v1

Version of Record: A version of this preprint was published at Optical and Quantum Electronics on August 14th, 2021. See the published version at https://doi.org/10.1007/s11082-021-03158-6.

Broadband reflector based on double-layer subwavelength gratings

Qi Wang*, Rui Li, Xufeng Gao, Shuhua Cao, Chunxian Tao, Ruijin Hong, and Dawei Zhang

Shanghai Key laboratory of Modern Optics System, Engineering Research Center of Optical Instrument and System, Ministry of Education and Shanghai Key Laboratory of Modern Optical System, School of Optical-Electrical and Computer Engineering, University of Shanghai for Science and Technology, 516 Jungong Rd, Shanghai 200093, China

Corresponding author: shelly3030@163.com (Qi Wang)

Abstract

A broadband reflector with a reflectance up to 97.8% over a 144 nm spectral range from 1476 to 1620 nm was proposed by comprising double-layer subwavelength gratings with one grating layer embedded in SiO_2 layer. An analysis of the resonance leaky modes with overlapping gratings showed the physical mechanism of the wide broad high-reflectivity band. The structural parameter tolerance was analyzed and the variation of bandwidth was explained by combining the behaviors of the two guided mode resonances. The guided mode resonance and high refractive index contrast properties led to a good angular tolerance that exhibited an angular insensitivity (~11°) at 1550 nm. Overall, the broadband reflector may benefit the monolithic integration of optoelectronic devices.

Keywords broadband reflector · guided mode resonance · double-layer grating

1. Introduction

Broadband reflectors with a high reflectance are used extensively in many applications, such as lasers (Chung 2015), sensors（Learkthanakhachon et al. 2016）, and polarizers (Mutlu et al. 2012). Because each guided mode resonance (GMR) is associated with 100% reflection, many methods that vary the structure of the waveguide grating have been used to design the broadband reflector. For example, in 2004, a broadband reflector at 1550 nm ($\Delta\lambda/\lambda > 35\%$, $R > 98.5\%$) was designed and verified by using the subwavelength grating (SWG) with a low-index sublayer (Mateus et al. 2004; Mateus et al. 2004). In 2008, Magnusson revealed the physical mechanism that yields a wide reflection band with a high reflectivity by using the enhancement reflection of multiple GMRs (Magnusson et al. 2008). A large-refractive-index grating that was suspended in air, namely, high-contrast-grating (HCG) can provide a wideband reflection (Chang-Hasnain et al. 2010). However, it is not easy to fabricate the suspended grating because of the lack of substrate.

Perfect reflectors that have a wideband, polarization independent, and omnidirectional are requested for expected in photonics and optical communications. However, the structure of a single-layer grating was not easy to be designed with these multiple properties. Comparatively, it is easier to be realized by using multilayer gratings. For example, two orthogonal gratings were demonstrated experimentally, and achieved a broad independent polarized bandwidth with a high reflectance (Niraula et al. 2016;

Ko et al. 2017). Nevertheless, it is difficult to combine separate SWGs compactly. More recently, a structure that consists of double-layer SWGs with different periods and fill factors based on GMR was proposed as broadband reflectors (Zhang et al. 2020), where an ultra-broadband reflection with a reflectance that exceeds 97% over a wavelength range of 955 nm in the near-infrared region was achieved. However, grating with a large fill factor increased the fabrication difficulty.

In this work, we designed double-layer subwavelength gratings with one grating layer embedded in an SiO_2 layer. In Section 2, a resonance pair overlap extends the reflection bandwidth. In Section 3, by varying the structural parameters, such as the homogeneous layer thickness and grating fill factor, the important effect of the two corresponding GMRs for the broad reflection band was discussed in detail, which tunes the bandwidth. An incident angle tolerance of ~ 11° at a central wavelength of 1550 nm was also analyzed.

2. Design and theory

The investigated broadband reflector was designed by double-layer subwavelength gratings and by applying a rigorous coupled-wave analysis method (Peng et al. 1995). The structure diagram is shown in Fig. 1a. The optimal structure consists of a fused silica substrate (n_1= 1.45), a 1000 nm fused silica spacer layer (n_1=1.45), and two silicon grating layers that include that the top silicon/air grating (n_H=3.48, n_L=1, b=190 nm) and the bottom silicon/ fused silica grating (n_H=3.48, n_L=1.45, b=190 nm). The grating period had Λ=800 nm, and the filling factor was f = 0.625. The incident wave was a transverse electric (TE) polarized wave (electric-field vector lies along the y-axis) at normal incidence.

In the simulation by finite-difference time-domain software (FDTD Solutions), boundary conditions of the domain along the y-axis were periodic, and the distance from the left to the right boundary was accurately equal to one grating period. Perfect match layers were used as boundaries at the top and bottom of the domain.

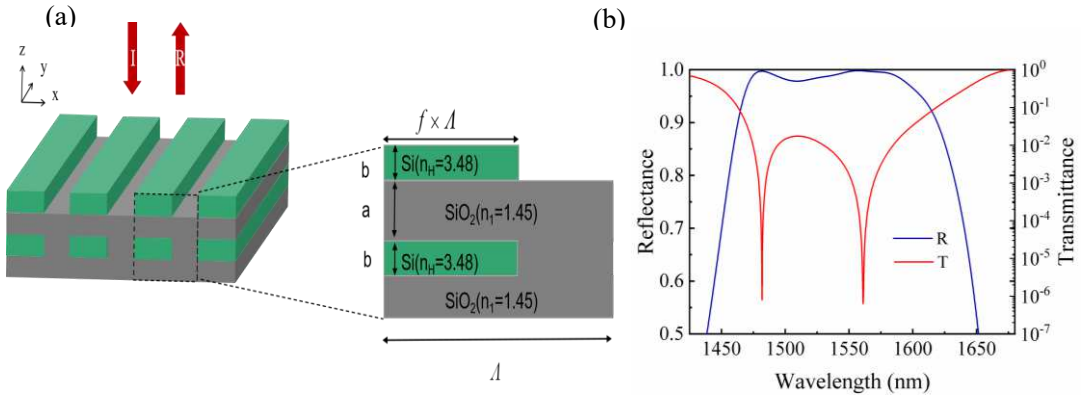

Fig.1 **a** Schematic view of the designed structure. The upper and lower Si gratings are separated by SiO_2 film layer, and the lower grating is embedded in the SiO_2 layer. The structural parameters are n_H =3.48, b=190 nm, Λ=800 nm, f = 0.625, n_1=1.45, and a=1000nm. I represents the incident plane wave, and R denotes reflected light. **b** Reflectance spectra on linear scale and transmittance spectra on logarithmic scale of the reflector normally illuminated by TE polarized wave. And the resonance wavelengths are 1481.84 and 1561.13 nm, respectively.

Under subwavelength conditions, high-order diffracted waves apart from the zeroth diffracted wave become evanescent waves. They propagate in the waveguide layer because they satisfy the phase-matching conditions with a guided mode. Due to the existence of a grating layer, they leak and interact with the zeroth diffracted wave to excite the resonance peak (Fan et al. 2019).

When the incident wave couples to a leaky waveguide mode by phase matching with the grating (Ding et al. 2007), the reflector works under a GMR. The subwavelength and phase-matching conditions under the general incident conditions are given by:(Ding et al. 2004)

$$\Lambda < \frac{\lambda}{n_c sin\theta + \max(n_c, n_s)} \tag{1}$$

$$\beta_m = k_0 \left(n_c \sin\theta - \frac{m\lambda}{\Lambda} \right), m = \pm 1, \pm 2, \ldots\ldots \tag{2}$$

where β_m denotes the propagation constant of the mth guided mode, which relates the diffraction order (m), the wave vector (k_0) in free space, and $k_0 = 2\pi/\lambda$. The incident angle (θ) is critical in the formation of resonant behavior. In the designed model, n_s is the refractive index of the fused silica substrate ($n_s = n_1 = 1.45$), and n_c is the refractive index of the cover ($n_{air} = 1$). By using the effective medium theory (EMT), the grating layer can be equivalent to a uniform waveguide layer with a certain effective refractive index (Brundrett et al. 1994). For the TE wave, the effective refractive index (n_g) can be expressed as Eq.(3).

$$n_g = [\varepsilon_{0,TE} + \frac{\pi^2}{3} f^2 (1-f)^2 (\varepsilon_H - \varepsilon_L)^2 (\frac{\Lambda}{\lambda})]^{\frac{1}{2}} , \tag{3}$$

where $\varepsilon_H = n_H^2$, $\varepsilon_L = n_L^2 = n_c^2$, and $\varepsilon_{0,TE}$ is the zero-order permittivity of the TE modes with $\varepsilon_{0,TE} = n_H^2 f + n_L^2 (1-f)$.

In the subwavelength region, because the structure is equivalent to the thin-film structure, the double-layer subwavelength gratings structure can be equivalent to a double-channel waveguide. Based on the slab waveguide theory (Zhang et al. 2006; Wang et al. 2016; Marcuse et al.1974), the transverse electric field of the double-channel waveguide for the TE mode can be described by:

$$E_y(z) = \begin{cases} A_0 \exp(p_0 z), & z < 0 \\ A_2 exp[i\kappa_2 (z-b)] + B_2 exp[-i\kappa_2 (z-b)], & 0 < z < b \\ A_1 exp[i\kappa_1 (z-b-a)] + B_1 exp[-i\kappa_1 (z-b-a)], & b < z < b+a \\ A_3 exp[i\kappa_3 (z-2b-a)] + B_3 exp[-i\kappa_3 (z-2b-a)], & b+a < z < 2b+a \\ A_1' exp[-p_1 (z-2b-a)], & 2b+a < z < +\infty \end{cases} , \tag{4}$$

where p_0, κ_1, κ_2, κ_3, and p_1 are the wavenumbers of the cover, the middle spacer layer, the top grating layer, the bottom grating layer, and the substrate in the z-direction, respectively. That is,

$$\kappa_1 = (k_0^2 n_1^2 - \beta^2)^{\frac{1}{2}}, \tag{5}$$

$$\kappa_2 = (k_0^2 n_{gt}^2 - \beta^2)^{\frac{1}{2}}, \tag{6}$$

$$\kappa_3 = (k_0^2 n_{gb}^2 - \beta^2)^{\frac{1}{2}}, \tag{7}$$

$$p_0 = (\beta^2 - k_0^2 n_c^2)^{\frac{1}{2}}, \tag{8}$$

$$p_1 = (\beta^2 - k_0^2 n_1^2)^{\frac{1}{2}}, \tag{9}$$

where n_{gt} and n_{gb} denote the effective refractive index of the top grating layer and the bottom grating layer, respectively. β represents the propagation constant of the waveguide mode, and $\beta \to \beta_m$.

Based on the continuity condition of E_y and $\partial E_y / \partial z$ at boundaries $z = 0$, $z = b$, and $z = a+b$, and $z = a+2b$, the dispersion equation of the double-layer gratings structure can be given by:

$$KH = v\pi + \arctan(p_0/K) + \arctan(p_1/K), \tag{10}$$

where K is determined by the eigenvalue equation of the matrix form, and $H = a + 2b$.

To clearly understand that a broadband reflection spectrum results from the appropriate coupling of two gratings and indicates the physical mechanism of a wideband, Fig.1b shows the reflection spectrum (linear scale) and transmittance spectra (logarithmic scale) of the designed structure under TE polarization. A broad-band reflector with reflectance > 97.8% over a 144 nm spectral range from 1476 to 1620 nm can be obtained at 1550 nm. Two transmittance dips exist inside the high reflectance band, which are located at 1481.84 and 1561.13 nm, respectively, and each of which corresponds to a GMR (Magnusson et al. 2008). The dips in the transmittance spectrum verify the presence of leaky-mode resonances, which is the physical basis of wideband reflectors (Shokooh-Saremi et al. 2010). The strong evanescent coupling between the two gratings splits the resonance, which leads to two strong transmission peaks near λ = 1500 nm (Sang et al. 2011). A reflection band at λ = 1500 nm is provided due to the overlapping of the GMRs. This result implies that the co-existence of the two TE leaky modes occurred because of the high refractive index difference between the materials and the profile modulation of the grating layer, and their interaction led to the formation of a broadband reflection spectrum (Sang et al. 2011). Overall, this high-reflection band is supported by a blend of two leaky modes (He et al. 2019; Shokooh-Saremi et al. 2008). However, the relative distance of the two GMRs is larger (Khaleque et al. 2014) and results in that a slight dip of high reflectivity near 1520 nm in the operating wavelength band, so the broadband is not flat enough (Sang et al. 2009). Nevertheless, a large relative separation between the two GMRs also contributes to the high extended reflectance band.

To gain insights into the broadband properties that arise from the coupling between the two GMRs, the normalized electric field intensity distribution at the resonant wavelengths of 1485.76 and 1515.65 nm is investigated in Fig.2a and b, respectively. The electric field distributions were localized on the grating ridge of the top grating and were highly enhanced. The narrower GMR spectral bandwidth is, yielded a higher normalized amplitude of the electric field enhancement effect (Wei et al. 2006). Because the peak at 1485.76 nm had a narrower linewidth than that at 1515.65 nm, the normalized amplitude of the electric field for the former was higher than that of the latter.

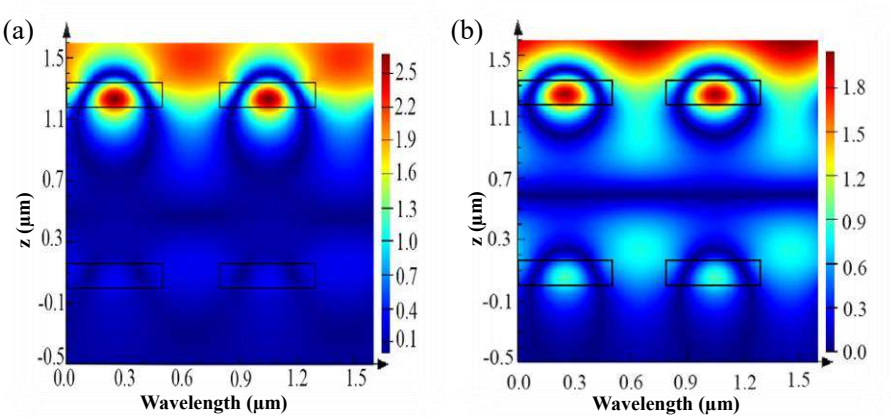

Fig.2 a and **b** Electric field distribution in plane y = 500 nm at resonance wavelengths λ = 1481.84 nm and λ = 1561.13 nm, respectively. Black lines are structural outlines, and two periods are illustrated. Structure parameters are the same as in Fig. 1.

3. Tolerance discussions

A prefabrication analysis of performance that is associated with parametric tolerance is required. In the following discussion, we show a design tolerance by varying the structure parameters, while keeping the others parameters constant. The reflectivity spectra for structure with different fused silica spacer thickness was calculated and is shown in Fig.3a. The sideband reflection at the longer wavelength varies more significantly than that at the shorter wavelength. Therefore, the reflection band at a longer wavelength side depends mostly on the middle spacer thickness (Yamada et al. 2017). To illustrate the physical mechanism, Fig. 3b compares the reflection spectra and transmittance dips for two spacer thicknesses (1000 and 1040 nm). The reflectivity bandwidth decreases when the fused silica spacer thickness is decreased. It can partially arise from the transmittance on logarithmic scale decreased (Sang et al. 2019). Therefore, an effective way of controlling the bandwidth of the reflection band can be obtained by changing the middle spacer thickness. Furthermore, in Fig.3c, the map R (b, λ) drawn wavelength versus spacer thickness directly illustrates the broadband extended relative to the increasing spacer thickness.

Fig.3d shows the spectra of the wideband reflection as a function of the grating fill factor. The change in grating fill factor shifts the reflection band to a shorter wavelength but has a negligible effect on the reflection band at a longer wavelength. The reflection band at a shorter wavelength produces a red-shift because the effective refractive index of the grating layer from the grating fill factor of the increases (Liu et al. 2010). The physical mechanism of the broadband reflector from the overlapping of the leaky mode resonance of two GMRs shows that, as the fill factor increases, the location of the two GMRs is red-shifted as shown in Fig.3e, which contributes to the wideband redshift. Fig.3f provides a reflection map of the wavelength versus fill factor, which shows that the broadband extended with a decreased in fill factor.

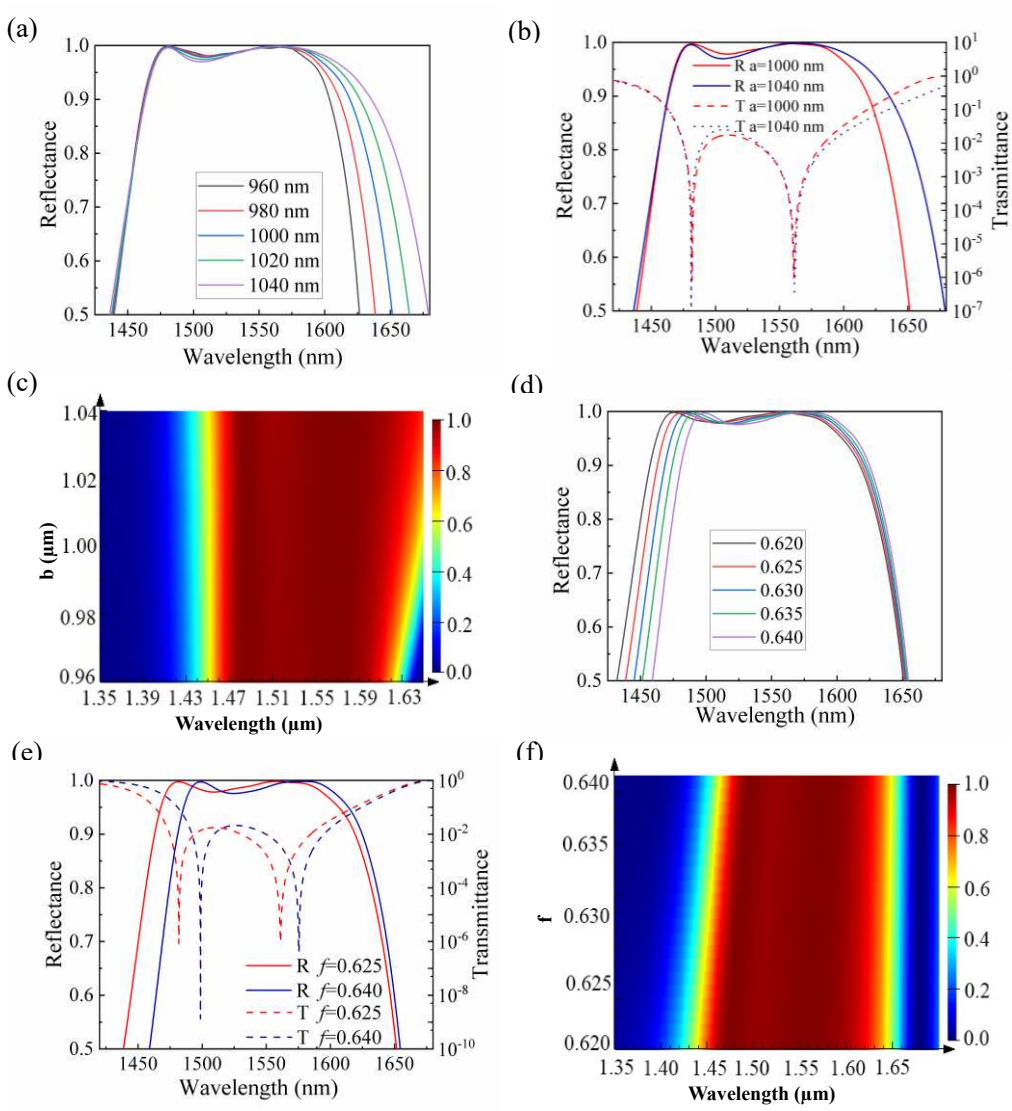

Fig.3 Reflectance spectra for middle fused silica spacer thickness **a** and fill factor of two silicon gratings **d**, while the remaining parameters are the same as those in Fig.1**a**. **b** and **e**and corresponding transmittance spectra on a logarithmic scale of the reflector. Reflection map for reflection for the middle spacer thickness **c** and fill factor of two silicon gratings **f**.

Fig.4a shows the angular robustness of the reflector. When the incident angle was increased with a 5° step interval, the high reflectance bandwidth narrows and shifts to a short wavelength with a deeper interceding reflection dip. Particularly, when the incident angle increases to 20°, an obvious reflection dip at ~1420 nm arises from a breakdown in the degeneracy of the guided mode resonances (Sang et al. 2009; Han et al. 2020), which reduces the GMRs' interaction and overlap. Therefore, when the incident angle deviates from normal incidence, the resonances split (Wang et al. 1993), which results in the decrease in reflectivity in the reflection band.

We examine the tolerance of the broadband spectra to a variation in incident angle, θ at 1550 nm is quantified in Fig. 4b. A high reflectivity (R > 99%) broadband exists from -11° to 11°, which means that the variation in incident angle within this range has an

almost negligible effect on the reflection spectra in the wavelength range of interest, which is useful in the application of the device. These large angular tolerances at a central wavelength of 1550 nm occur mainly because of the blend of the two GMRs (Huang et al. 2016).

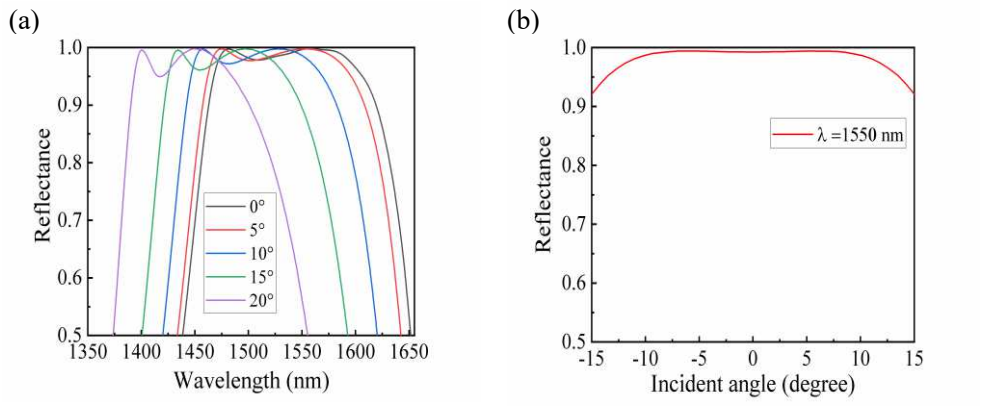

Fig.4 a Reflectance spectra as a function of the incident angle, while the remaining parameters are the same as those in Fig.1**a**. **b** angular behavior of the reflector at 1550 nm. It can achieve high reflectivity (R>99%) at the range of -11° to 11°.

4. Conclusions

We demonstrated a broadband reflector based on double-layer subwavelength gratings with an identical period and fill factor, which exhibited a reflection spectrum (above 144 nm) and centered at 1550 nm with a high reflectance (R > 97.8%) and a good angular insensitivity (~ 11°) at 1550 nm. The physical mechanism can be explained by the interactions of two GMRs. The tolerance analysis implies that the demonstrated reflector had a reasonably good fabrication tolerance. The broadband reflector has potential application in areas where a high reflectance is required, impart of the double-layer resonance structures with an increase in degrees of design freedom, and facilitates monolithic integration of optoelectronic devices for a wide range of wavelengths.

Declaration

Conflict of Interest The authors declare no conflicts of interest.

References

Brundrett, D.L., Glytsis, E.N., Gaylord, T.K., Homogeneous layer models for high-spatial-frequency dielectric surface-relief gratings: conical diffraction and antireflection designs, *Appl. Opt.* 33, 2695-2706 (1994)

Chang-Hasnain, C.J., High-contrast gratings as a new platform for integrated optoelectronics, *Semicond. Sci. Technol*. 26, 1-11 (2010)

Chung, I.-S., Study on differences between high contrast grating reflectors for TM and TE polarizations and their impact on VCSEL designs, *Opt. Express*. 23, 16730-16739 (2015)

Ding, Y., Magnusson, R., Band gaps and leaky-wave effects in resonant photonic-crystal waveguides, *Opt. Express.* 15, 680-694 (2007)

Ding, Y., MagnussonR., Doubly resonant single-layer bandpass optical filters, *Opt. Lett.* 29, 1135-1137 (2004)

Fan, L.N., Jia, K.H., Ma, J.S., Transmission filter controlled by incident conditions in single-layer waveguide grating structures, *Appl. Opt.* 58, 8371-8375(2019)

Han, S., Rybin, M.V., Pitchappa, P., Srivastava, Y.K., Kivshar, Y.S., Singh, R., Guided-Mode Resonances in All-Dielectric Terahertz Metasurfaces, *Adv. Opt. Mater.* 8, 1900959 (2020)

He, S.M., Liu, Q.F., Sa, T.L., Wang, Z.H., Design of broadband reflector at the visible wavelengths using particle swarm optimization, *Aip Adv.* 9, 075301 (2019)

Huang, L., Liang, D., Zeng, J., Xiao, Y., Wu, H., Xiao, W., A silicon-based wideband multisubpart profile grating reflector, *Opt Laser Technol.* 78, 79-82 (2016)

Khaleque, T., Uddin, M.J., Magnusson, R., Design and fabrication of broadband guided-mode resonant reflectors in TE polarization, *Opt. Express.* 22, 12349-12358 (2014)

Ko,Y.H., Lee, K.J., Magnusson, R., Experimental demonstration of wideband multimodule serial reflectors, *Opt. Express.* 25, 8680-8869 (2017)

Learkthanakhachon, S., Taghizadeh, A., Park, G.C., Yvind, K., Chung, I.-S., Hybrid III-V/SOI resonant cavity enhanced photodetector, *Opt. Express.* 24, 16512-16519 (2016)

Liu, W., Lai, Z., Guo, H., Liu, Y., Guided-mode resonance filters with shallow grating, *Opt. Lett.* 35, 865-867 (2010)

Magnusson, R., Shokooh-Saremi, M., Physical basis for wideband resonant reflectors, *Opt. Express.* 16, 3456-3462 (2008)

Marcuse, D.M., Theory of dielectric optical waveguides, 2nd ed., Academic Press, New York, NY, USA, (1974)

Mateus, C.F.R., Huang, M.C.Y., Chen, L., Chang-Hasnain, C.J., Suzuki, Y., Broad-band mirror (1.12-1.62 μm) using a subwavelength grating, *IEEE Photonics Technology Letters.*16, 1676-1678 (2004)

Mateus, C.F.R., Huang, M.C.Y., Deng, Y.F., Neureuther, A.R., Chang-Hasnain, C.J., Ultrabroadband mirror using low-index cladded subwavelength grating, *IEEE Photonics Technology Letters.* 16, 518-520 (2004)

Mutlu, M., Akosman, A.E., Ozbay, E., Broadband circular polarizer based on high-contrast gratings, *Opt. Lett.* 37, 2094-2096 (2012)

Niraula, M., Magnusson, R., Unpolarized resonance grating reflectors with 44% fractional bandwidth, *Opt. Lett.* 41, 2482-2485 (2016)

Peng, S., Morris, G.M., Efficient implementation of rigorous coupled-wave analysis for surface-relief gratings, *J. Opt. Soc. Am. A.* 2532, 1087-1096 (1995)

Sang, T., Cai, T., Cai, S., Wang, Z., Tunable transmission filters based on double-subwavelength periodic membrane structures with an air gap, *J. Opt.* 13, 937-946 (2011)

Sang, T., Gao, J., Yin, X., Qi, H.L., Wang, L., Jiao, H.F., Angle-Insensitive Broadband Absorption Enhancement of Graphene Using a Multi-Grooved Metasurface, *Nanoscale. Res. Lett.* 14, 105-105 (2019)

Sang, T., Wang, L., Ji, S., Ji, Y., Wang, Z., Systematic study of the mirror effect in a poly-Si subwavelength periodic membrane, *J. Opt. Soc. Am. A.* 26, 559-565 (2009)

Shokooh-Saremi, M., Magnusson, R., Wideband leaky-mode resonance reflectors: Influence of grating profile and sublayers, *Opt. Express.* 16, 18249-18263 (2008)

Shokooh-Saremi, M., Magnusson, R., Leaky-mode resonant reflectors with extreme bandwidths, *Opt. Lett.* 35, 1121-1123 (2010)

Wang, S.S., Magnusson, R., Theory and applications of guided-mode resonance filters, *Appl. Opt.* 32, 2606-2613 (1993)

Wang, X.P., Cheng, Y., Cao, Z.Q., Progress in Planar Optical Waveguides, Shanghai Jiao Tong University Press, Shanghai,China, (2016)

Wei, C., Liu, S., Deng, D., Shen, J., Shao, J., Fan, Z., Electric field enhancement in guided-mode resonance filters, *Opt. Lett.* 31, 1223-1225 (2006)

Yamada, K., Lee, K.J., Ko, Y.H., Inoue, J., Kintaka, K., Ura, S., Magnusson, R., Flat-top narrowband filters enabled by guided-mode resonance in two-level waveguides, *Opt. Lett.* 42, 4127-4130 (2017)

Zhang, J., Luo, K.J., The Improvement of TE Mode Transfer Matrix and Modes Latent Equation in Multi-Channel Optical Wave-Guide, *Journal of Jiangxi Normal University.* 30, 355-357 (2006)

Zhang, J.L., Shi, S.K., Jiao, H.F., Ji, X.C., Wang, Z.S., Chen, X.B., Ultra-broadband reflector using double-layer subwavelength gratings, *Photon. Res.* 8, 426-429 (2020)

Figures

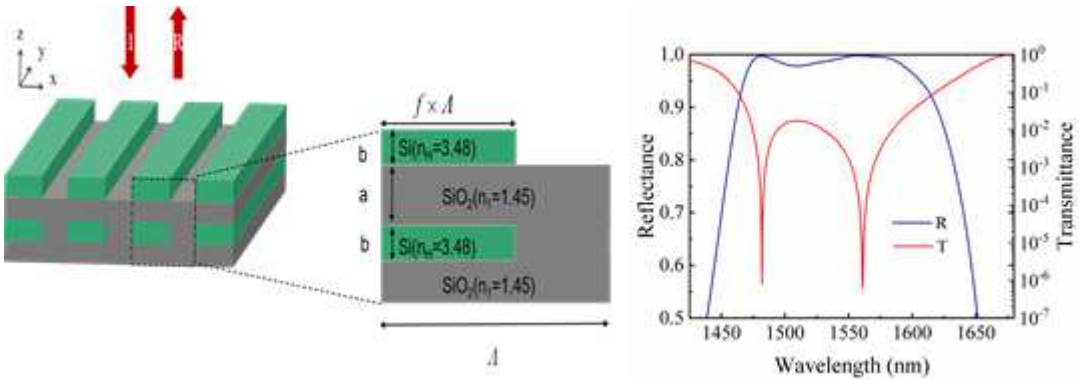

Figure 1

a Schematic view of the designed structure. The upper and lower Si gratings are separated by SiO2 film layer, and the lower grating is embedded in the SiO2 layer. The structural parameters are nH =3.48, b=190 nm, Λ=800 nm, f = 0.625, n1=1.45, and a=1000nm. I represents the incident plane wave, and R denotes reflected light. b Reflectance spectra on linear scale and transmittance spectra on logarithmic scale of the reflector normally illuminated by TE polarized wave. And the resonance wavelengths are 1481.84 and 1561.13 nm, respectively.

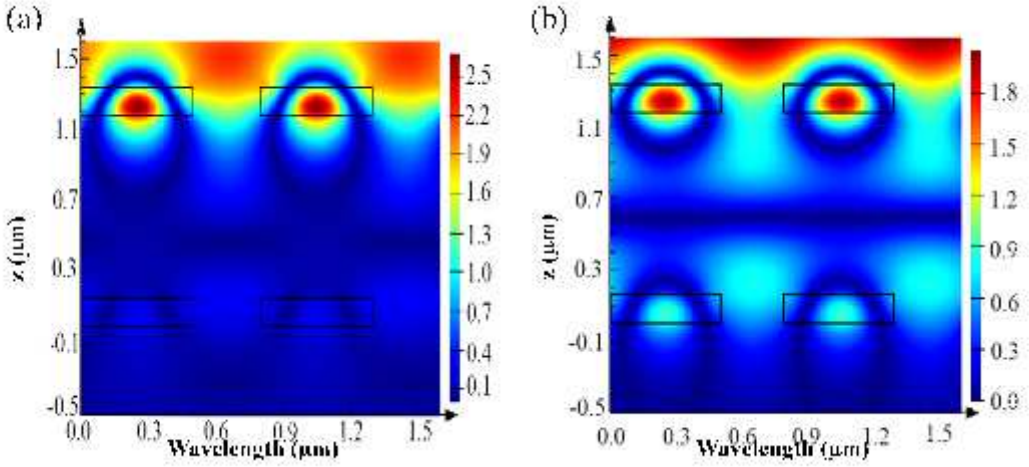

Figure 2

a and b Electric field distribution in plane y = 500 nm at resonance wavelengths λ = 1481.84 nm and λ = 1561.13 nm, respectively. Black lines are structural outlines, and two periods are illustrated. Structure parameters are the same as in Fig. 1.

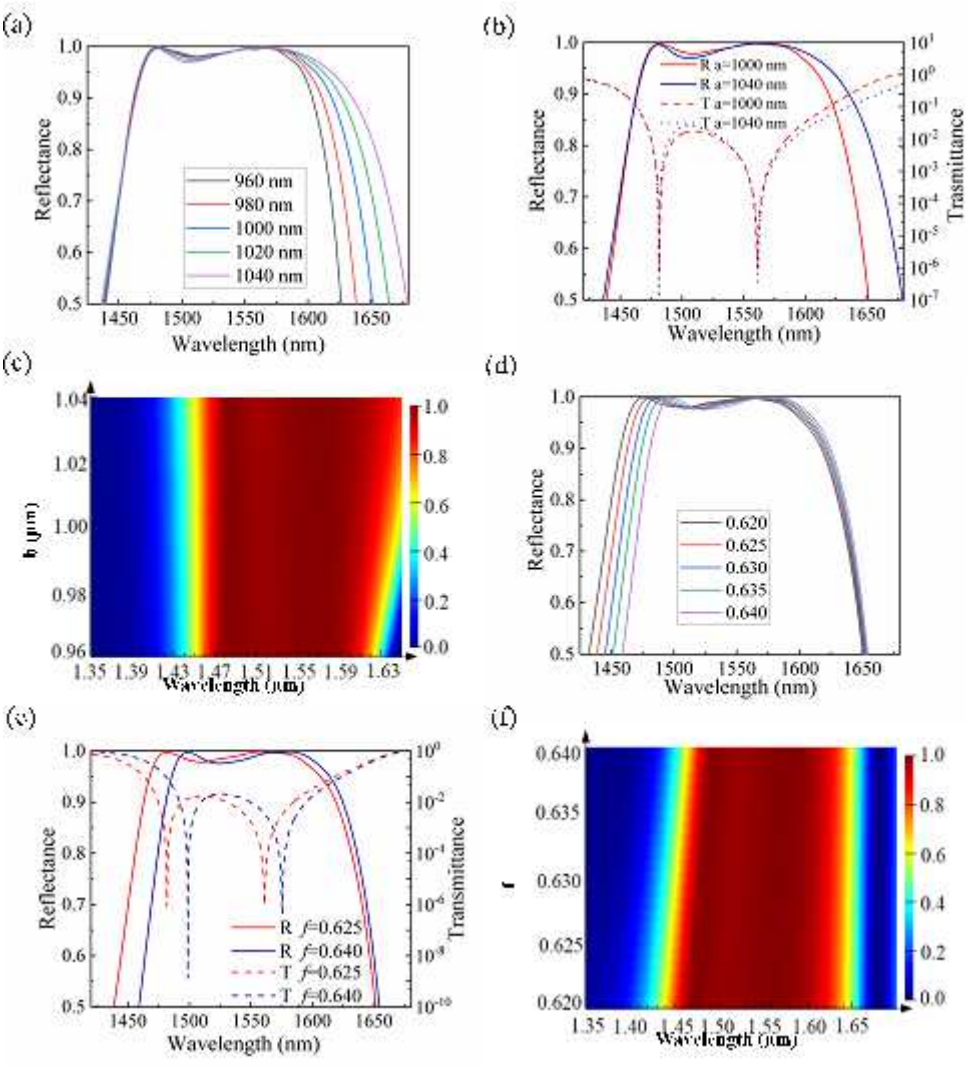

Figure 3

Reflectance spectra for middle fused silica spacer thickness a and fill factor of two silicon gratings d, while the remaining parameters are the same as those in Fig.1a. b and eand corresponding transmittance spectra on a logarithmic scale of the reflector. Reflection map for reflection for the middle spacer thickness c and fill factor of two silicon gratings f.

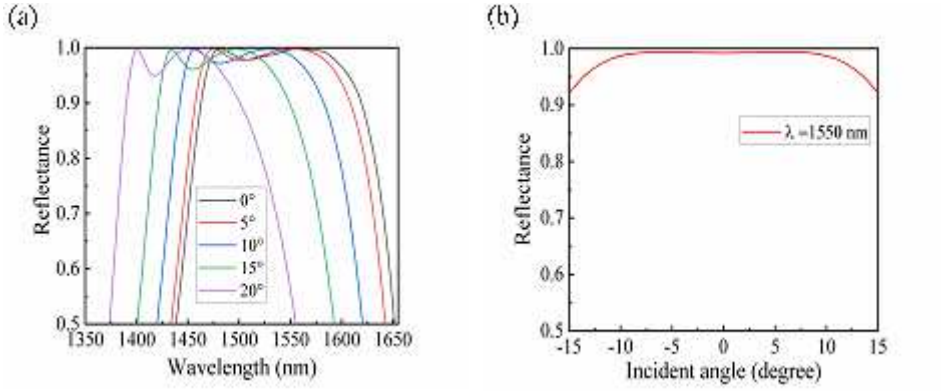

Figure 4

Reflectance spectra as a function of the incident angle, while the remaining parameters are the same as those in Fig.1a. b angular behavior of the reflector at 1550 nm. It can achieve high reflectivity (R>99%) at the range of -11° to 11°.